

PAPER

## Magnetism of $\text{Bi}_2\text{Se}_3$ thin films with Eu-rich flat inclusions

To cite this article: L N Oveshnikov *et al* 2018 *J. Phys.: Condens. Matter* **30** 445801

View the [article online](#) for updates and enhancements.




**IOP | ebooks™**

Bringing you innovative digital publishing with leading voices to create your essential collection of books in STEM research.

Start exploring the [collection](#) - download the first chapter of every title for free.

# Magnetism of $\text{Bi}_2\text{Se}_3$ thin films with Eu-rich flat inclusions

L N Oveshnikov<sup>1,2</sup> , Ya I Rodionov<sup>3,4</sup>, K I Kugel<sup>3,5</sup>, I A Karateev<sup>1</sup>,  
A L Vasiliev<sup>1</sup>, Yu G Selivanov<sup>2</sup>, E G Chizhevskii<sup>2</sup>, I S Burmistrov<sup>6</sup>  
and B A Aronzon<sup>1,2</sup>

<sup>1</sup> National Research Center ‘Kurchatov Institute’, Moscow, 123182, Russia

<sup>2</sup> P N Lebedev Physical Institute, Russian Academy of Sciences, Moscow, 119991, Russia

<sup>3</sup> Institute for Theoretical and Applied Electrodynamics, Russian Academy of Sciences, Moscow, 125412, Russia

<sup>4</sup> National University of Science and Technology MISIS, Moscow, 119049, Russia

<sup>5</sup> National Research University Higher School of Economics, Moscow, 101000, Russia

<sup>6</sup> L D Landau Institute for Theoretical Physics, Russian Academy of Sciences, Chernogolovka, Moscow region, 142432, Russia

E-mail: [Oveshln@gmail.com](mailto:Oveshln@gmail.com)

Received 19 June 2018, revised 6 September 2018

Accepted for publication 12 September 2018

Published 10 October 2018



CrossMark

## Abstract

We report the results of experimental and theoretical studies of Eu-doped  $\text{Bi}_2\text{Se}_3$  thin films with extremely inhomogeneous distribution of magnetic component. The obtained electron microscopy images suggest that Eu atoms are concentrated within platelet-like nano-inclusions. The number of inclusions grows with the increase in Eu content,  $x$ . Moreover, at relatively high  $x$  values, the stacks of platelets (inclusions located one under another) become rather frequent. A comparative analysis of magnetic properties of the films under study reveals no pronounced changes of their temperature dependence with the increase in  $x$ , which, however, leads to the decrease in the average magnetic moment  $\mu_{\text{Eu}}$  per Eu atom. A theoretical analysis of different mechanisms contributing to a possible magnetic ordering in the Eu-doped films demonstrates that at small distances (i.e. within a platelet) a dominant contribution is related to the RKKY interaction via electrons in the bulk, while the ordering at inter-platelet distances is governed by magnetic dipole–dipole interaction. The latter implies the antiferromagnetic ordering within the stacks of platelets explaining a drop of  $\mu_{\text{Eu}}$  per Eu atom. We employ the model of a metallic spin glass to estimate the transition temperature, characterising the interaction within the ensemble of randomly distributed magnetic platelets. This estimate gives satisfactory agreement with the experiment, even if we take into account a finite film thickness, thus, neglecting the interaction anisotropy and including only the antiferromagnetism related to the stacking. While the overall contribution of interface Dirac electrons is damped in the systems under study, we argue that the obtained results can be used for the investigation of ultrathin films with analogous impurity profile, where this contribution should be clearly pronounced.

Keywords: topological insulators, magnetic impurities, RKKY interaction, magnetic dipole–dipole interactions, platelet inclusions, ferromagnetism, antiferromagnetism

(Some figures may appear in colour only in the online journal)

## 1. Introduction

In recent years, topological insulators (TI) [1–3] were thoroughly studied using a vast variety of experimental methods and various theoretical approaches. The basic interest in these systems stems from the unique properties of Dirac electrons, which are believed to be present in topologically nontrivial states at TI boundaries/interfaces (depending on the system dimensionality) with trivial media. Later on, it was realized that for some specific applications one needs to establish a ferromagnetic (FM) state in TI by introducing magnetic impurities. Although magnetic TIs (MTI) exhibit some striking phenomena (for example, quantum anomalous Hall effect [4]), they are much less studied than pure TIs. Thus, the investigations of magnetic TI systems are quite promising both for fundamental condensed matter physics and applications.

In almost all of MTI-related studies, the distribution of magnetic impurities in the TI matrix was assumed to be homogeneous. It allowed one to consider such system in terms of effective Hamiltonian yielding the opening of exchange gap at Dirac points when the system becomes ferromagnetic. The latter suggests that the topologically nontrivial states should eventually evolve to ordinary ones with the increase in the exchange gap. Usually this transition is monitored via the transport measurements. When exchange gap becomes sufficiently large, the phase shift of time-reversed electron waves in the interference loop (i.e. Berry phase) vanishes and antilocalization phenomena is replaced by weak localization, which is clearly seen in the experiment as sign change of low-field magnetoresistance [5, 6]. In this aspect, it is not of principal importance, where the magnetic subsystem is located—within TI film or near its boundaries, the qualitative behavior remains the same when one deals with the TI/ferromagnet interface [7]. A detailed study of the interaction of Dirac electrons with magnetic moments has revealed various more sophisticated effects. For example, a controllable spin-orbit torque device was proposed based on the idea of gate-induced interface imbalance [8]. On the other hand, the impact of Dirac electrons on the FM subsystem remains largely unstudied. Recently, interface Dirac electrons in ultrathin MTI films have been reported to be possibly responsible for the appearance of topological Hall effect. It is argued that at some critical thickness interface carriers may stabilize a skyrmion pattern [9]. Still it is not clear how the observed phenomena are affected by the gap opening due to hybridization of interface states at such small film thickness [10]. Thus, to create a self-consistent model of MTI properties, one needs to combine data on the system at different regimes (i.e. films with various thickness and magnetic doping level). Therefore, we limit ourselves to the case of relatively thick films. It can be used to establish a basic picture for investigation of the system evolution with decreasing thickness (e.g. to elucidate effects driven by the Dirac electrons at the interfaces).

In this work, we study  $\text{Bi}_2\text{Se}_3$  film samples doped by europium. It worth mentioning that atomic magnetic moment of Eu is  $7/2$ , which is considerably higher than those of 3-d metals commonly used as dopants in MTI systems. Thus, a higher local magnetic field can be achieved at lower impurity

concentrations, providing higher crystalline perfection of the film. Here, the most interesting case is that of the dilute limit (having some similarities with dilute magnetic semiconductors), when the distance between the homogeneously distributed magnetic impurities is much larger than the lattice spacing. However, the actual situation turns out to be even more fascinating. The electron microscopy provides a clear evidence that even at low density of Eu impurities, Eu becomes segregated into nanoscale platelet inclusions within the host  $\text{Bi}_2\text{Se}_3$  material. Hence, we are dealing with extremely inhomogeneous distribution of Eu magnetic momenta. Moreover, at low temperatures, the inclusions are FM themselves and their magnetic moments can be treated as a kind of superspins interacting with each other. Thus, in the system under study, the magnetism of topological insulators becomes combined with rather topical problems widely studied in the systems of magnetic nanoparticles [11]. In terms of applications, our transport studies suggest that topological states at the film interfaces (with the substrate and capping layer) are rather robust with respect to local magnetic fields, thus, a particular inclusion may open a gap only in a finite surface region. In this way, it is possible to realize lateral TI/MTI heterostructures or even superlattices. The films under study represent a prototype spontaneously formed heterostructure of this kind. Therefore, such systems can be promising for the efficient control of emergent spin-polarized currents.

Moreover, in the dilute regime for studied films (corresponding to the case when the distance between magnetic platelets far exceeds their characteristic size), one usually expects that the interaction between magnetic inclusions is related to the Ruderman–Kittel–Kasuya–Yosida (RKKY) type indirect exchange interaction mediated by charge carriers [12–14]. Note that the RKKY interaction is described by a rapidly oscillating function with the period having the scale of Fermi wavelength. Nevertheless, if the chemical potential is small, the period of oscillations becomes larger than the inter-platelet distance, and the system generally exhibits a ferromagnetic pattern. In our case, the estimates show that the chemical potential cannot be considered as small. However, the experimental data clearly suggest that at low temperatures ( $<10$  K), the system undergoes the transition to the ferromagnetic state (or, at least, to that with rather long-range ferromagnetic correlations). Thus, we need to find out what mechanism controls this phase transition. This problem is addressed in detail in the last part of our paper.

The paper is organized as follows. In section 2, we describe our samples and experimental techniques. In section 3, we discuss the obtained experimental results with the main emphasis on the structural and magnetic characteristics of our samples. Section 4 contains the theoretical analysis of different mechanisms underlying the magnetic characteristics of the samples under study. Basically, we formulate the simplest model explaining the anomalies in the observed magnetic response, taking into account the specific distribution of Eu atoms within  $\text{Bi}_2\text{Se}_3$  host material. The concluding remarks are given in section 5. Some mathematical details alongside with additional estimations are addressed in the appendix.

## 2. Samples and experimental setup

It is worth mentioning that Eu doping of  $\text{Bi}_2\text{Se}_3$  have not been studied earlier by other groups, although such magnetic doping is quite natural from the viewpoint of the Se-based TIs since EuSe is a well-known FM semiconductor [15]. The Eu-doped  $\text{Bi}_2\text{Se}_3$  thin films were synthesized by the molecular-beam epitaxy technique using evaporation cells with binary  $\text{Bi}_2\text{Se}_3$  source as well as cells with elemental Bi, Se, and Eu. More detailed description of the growth process and structural characterization of studied films can be found in [16, 17]. For simplicity, we can consider our films as ternary  $(\text{Bi}_{1-x}\text{Eu}_x)_2\text{Se}_3$  compounds and use  $x$  as a measure of Eu content. Obtained films ( $x = 0.038, 0.07, 0.13, 0.21$ ) with the thickness from 20–60 nm were cleft into small pieces for structural, magnetic, and transport measurements.

The films were studied using the scanning/transmission electron microscope (S/TEM) Titan 80-300 (FEI, US) operated at 300 kV and equipped with the spherical aberration (Cs) corrector (electron probe corrector), high-angle annular dark-field detector, atmospheric thin-window energy dispersive x-ray (EDX) spectrometer (Phoenix System, EDAX, US), and post-column Gatan energy filter (Gatan, US). The cross-section specimens were prepared by the standard focus ion beam procedure in Helios (FEI, USA) dual beam instrument.

Magnetic properties of Eu-doped  $\text{Bi}_2\text{Se}_3$  films were studied within the  $T = 2\text{--}65$  K temperature range in the applied magnetic field up to  $H = 70$  kOe using a superconducting quantum interference device magnetometer MPMS (Quantum Design, USA).

## 3. Experimental results

As it was reported earlier [16, 17], the distribution of magnetic atoms within the  $\text{Bi}_2\text{Se}_3$  host in the films under study is highly inhomogeneous, namely Eu atoms are concentrated within distinct regions forming platelet inclusions observed in TEM images as dark stripes (figure 1(a)). The concentration and mean size of the platelets increase with the Eu content.

The EDX spectroscopy data suggest that Eu atoms are distributed only within such platelet inclusions, whereas the rest part of the film does not contain a detectable amount of Eu. For all studied films, we performed the EDX microanalysis from the areas similar to ones highlighted by red and blue rectangles shown in cross-section image of the specimen (figure 2(a)). Area 1 lies outside the platelet region, while area 2 includes a platelet. Obtained EDX spectra are shown in figure 2(b). It is clear that the spectrum for area 2 contains two distinct peaks related to the presence of Eu atoms, which are absent in spectrum for area 1 (i.e. there is no detectable amount of Eu atoms). Film composition outside the inclusions (area 1) is close to the stoichiometric  $\text{Bi}_2\text{Se}_3$ . It is worth mentioning that the peaks related to Cu atoms come from the copper sample holder used for TEM experiments.

At low  $x$  values, the Eu-rich inclusions are quite rare and can be considered as isolated ones. Introducing a single inclusion, in fact, preserves the high crystalline quality of

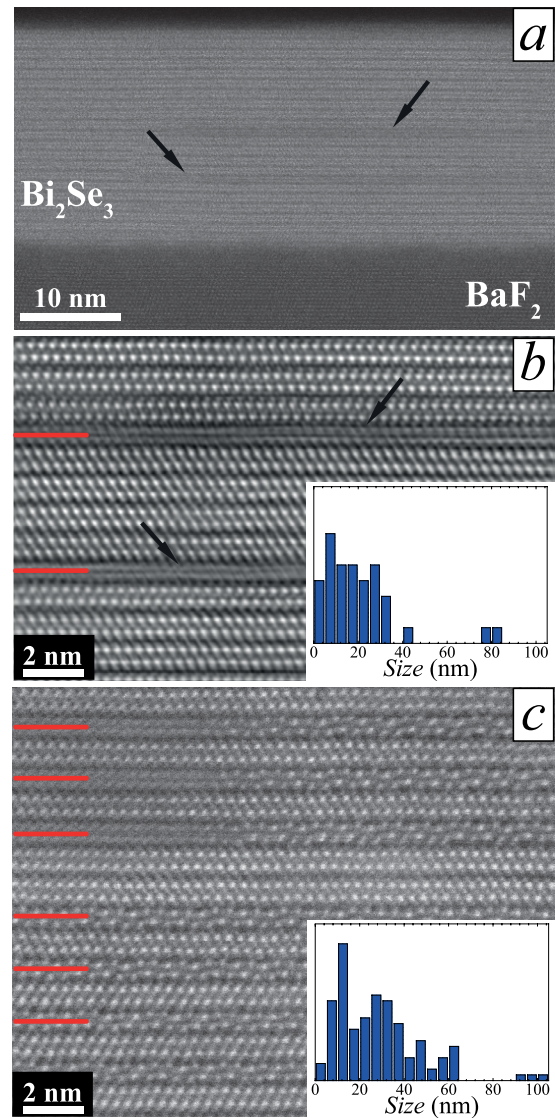


**Figure 1.** Electron microscopy results: (a) cross-section STEM image of sample with  $x = 0.038$ ; (b) HRSTEM image of inclusion regions in the sample with  $x = 0.038$ ; (c) HRSTEM image of inclusion regions in the sample with  $x = 0.21$ . Black arrows and red lines indicate flat Eu-rich inclusions (platelets). Insets of panels (b) and (c) show the corresponding platelet size distributions for these films.

surrounding  $\text{Bi}_2\text{Se}_3$  matrix (figure 1(b)). Due to the random spatial distribution of platelets, one can also observe stacks of them. Basically, this means that several platelets are located one under another. The spacing between the inclusions in a stack involves from one to several  $\text{Bi}_2\text{Se}_3$  quintlayers (figure 1(b)). It is important to note that at higher  $x$  values, the stacks include several platelets separated by only one  $\text{Bi}_2\text{Se}_3$  quintlayer (figure 1(c)). Thus, taking into account the stacking phenomena, our films can be considered as an ensemble of flat Eu-rich inclusions embedded into pure  $\text{Bi}_2\text{Se}_3$ .

The analysis of the shape and sizes of the 2D platelets was performed. The histograms of lateral dimensions of the platelets are presented in the insets of figures 1(b) and (c). The right sides of the images of the platelets shown in figure 1(c) demonstrate distinct contrast (well defined ordered structure),

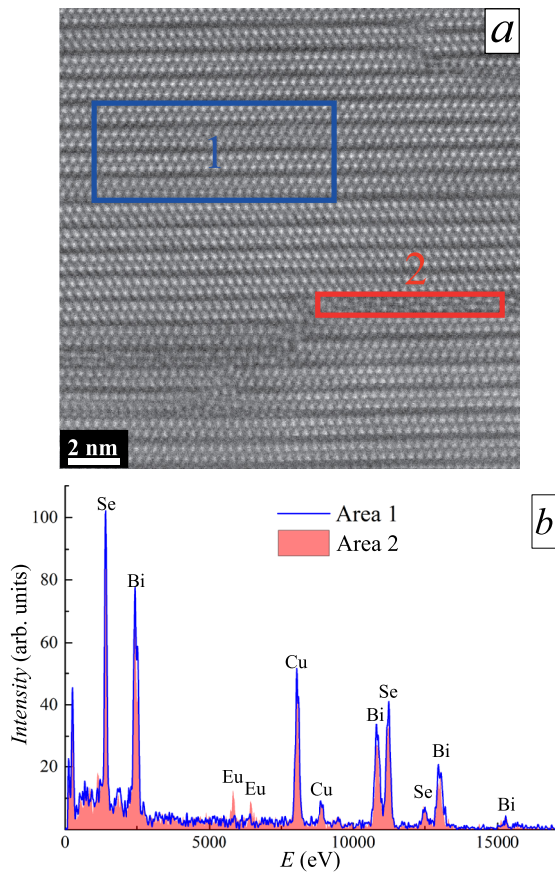


**Figure 2.** EDX spectroscopy results: (a) cross-section STEM image of sample with  $x = 0.07$ ; colored frames represent EDX scanning areas outside the platelet (area 1) and including the platelet (area 2); (b) corresponding EDX spectra for different scanning areas; the peaks are related to the various elements.

coming from atomic columns. Since the specimens thickness were between 20–40 nm, we believe that the dimensions of the platelets in the direction parallel to the e-beam are equal to the thickness of the sample. Our preliminary investigations of plan-view samples, which will be presented elsewhere, also demonstrated the isotropy of the platelets in lateral directions. Thus, we estimated the mean size values by calculating the simple weighted average of the size distribution histograms. Mean size gradually increases with the Eu content. Aside from the stacking phenomenon, the spatial distribution of platelets does not exhibit any particular pattern, thus it is assumed to be 2D uniform and the corresponding mean interplatelet distances are used for the estimates in the following sections.

The next step deals with the study of magnetic properties of our films. Generally, when we study thin films, the significant part of measured signal is related solely to the contribution of substrate due to the enormous difference in the thickness. Thus, the contribution related to the film itself is determined with a limited accuracy. Bearing this in mind, we, nevertheless, were able to distinguish a nonlinear contribution observed at low temperatures, which presumably corresponds to magnetic inclusions. This contribution saturates at low magnetic field (below 10 kOe) and even exhibits a small hysteresis. To describe the evolution of magnetic response

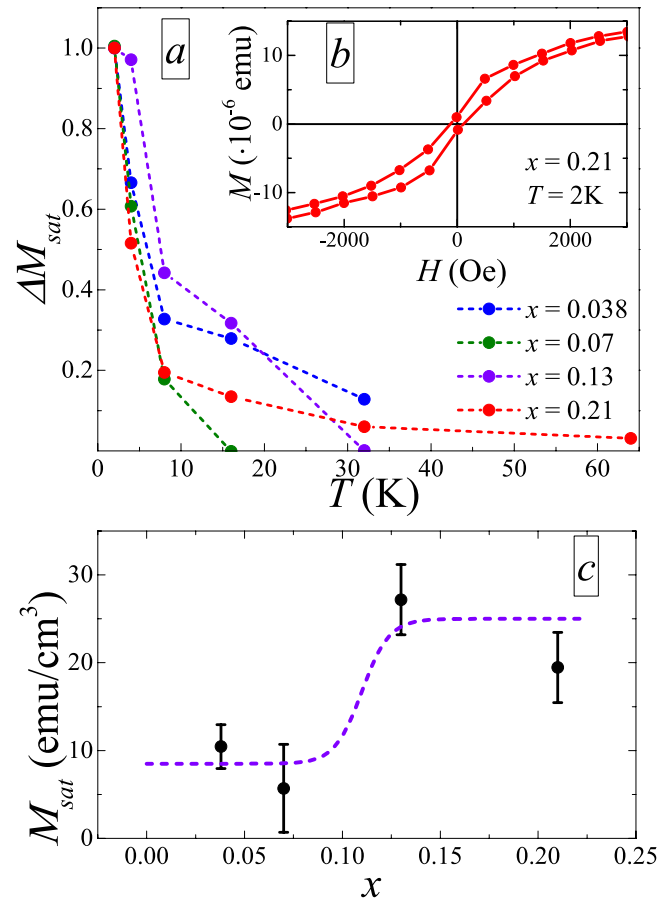


**Figure 3.** Magnetometry results: (a) temperature dependence of normalized saturation magnetic moment  $\Delta M_{\text{sat}} = M_{\text{sat}}(T)/M_{\text{sat}}(T = 2 \text{ K})$  for the studied films; (b) field dependence of magnetization for  $x = 0.21$  sample at 2 K, it demonstrates a distinct hysteresis loop in a weak-field region; (c) dependence of saturation magnetization (measured at  $T = 2 \text{ K}$ ) on Eu content. Dashed line is a guide to the eye representing a stepwise function (see the text).

of the films under study, we employed a rather straightforward approach. Assuming that the normalized magnetic moment corresponding to the saturation at given temperature,  $\Delta M_{\text{sat}} = M_{\text{sat}}(T)/M_{\text{sat}}(T = 2 \text{ K})$ , depends both on the number of inclusions (Eu content) and on the interactions between them, we plot the corresponding temperature dependence (see figure 3(a)). In the framework of such approach, the value of  $T_c$  corresponding to the onset of the long-range order can be related to the beginning of steep increase in  $\Delta M_{\text{sat}}(T)$ . It can be easily seen that the aforementioned increase remains to be rather smooth and can be attributed to the inhomogeneous distribution of inclusions (leading to the percolation-type behavior), and, despite the drastic increase in Eu content (from 0.038 to 0.21), the estimated  $T_c$  values do not change significantly. In particular, the estimation shows that the long-range order arises within the temperature range from 8 to 15 K. It is important to note that for the film with  $x = 0.21$  we have observed a distinct hysteresis loop with the coercivity of about  $\sim 120 \text{ Oe}$  (see figure 3(b)), which confirms a ferromagnetic ordering at low temperatures. Taking into account that the increase in Eu content leads to the growth

of platelets concentration without significant changes of their morphology, we suggest that these inclusions are FM, and the long-range order appears due to their interaction. At higher  $x$  values, this interaction gives FM ordering, while at low  $x$  the interaction between inclusions may, at least, create a correlated state that makes it easier to polarize magnetic moments of platelets by external field. The latter corresponds well to low values of saturation field (below 10 kOe) observed in the experiment.

If we plot the saturation magnetization versus Eu content (see figure 3(c)), we can see that this dependence has a roughly stepwise form. Basically, it corresponds to the percolation-type behavior of the exchange interaction, i.e. we have a small signal at low  $x$  that steeply grows after the percolation threshold and then saturates. As it was mentioned earlier, the form of  $M(T)$  dependence also suggests a percolative character associated with the random-like distribution of interacting platelets. Within simple percolation model the increase of  $M$  along with  $x$  seems to be quite anticipated.

However, if we express the magnetization in terms of the magnetic moment  $\mu_{\text{Eu}}$  per Eu atom, it becomes evident that the increase in Eu content, in average, leads to the decrease in  $\mu_{\text{Eu}}$  by a factor of  $\mu_{\text{Eu}}(x = 0.038)/\mu_{\text{Eu}}(x = 0.21) \approx 2.6$ . It is worth mentioning that absolute values of  $\mu_{\text{Eu}}$  for studied films are somewhat lower than tabulated value of 3.5 (magnetic moment of isolated  $\text{Eu}^{2+}$  ion), which can be related to a complex chemical structure of the inclusions (i.e. to the presence of  $\text{Eu}^{3+}$  ions with zero magnetic moment), that will be investigated in further studies. Nevertheless, it does not affect any results of the present paper since provided calculations deal only with the number of magnetic moments (i.e.  $\text{Eu}^{2+}$  ions) which can be reliably estimated from our data. Thus, we can formulate several interconnected experimental features: the drastic increase in the Eu content does not significantly affect the temperature range where the nonlinear contribution is observed, moreover, it leads to the decrease in magnetic moment per Eu atom, whereas the Eu-rich inclusions remain FM.

Before trying to give a theoretical interpretation to these features, we should note that based on our transport data for the studied films, we have performed some simple estimations (see appendix A.1). Comparing the transport parameters of the studied films to the results of other groups, we noticed that the values of charge carrier densities  $N_{\text{Hall}}$  deduced from the Hall effect (assuming that our films can be considered as purely 2D) are quite similar. Nevertheless, the obtained values  $N_{\text{Hall}} \approx (6-9) \times 10^{13} \text{ cm}^{-2}$  are still very high to be ascribed to a conventional 2D system. Considering our films as vessels for three groups of charge carriers (top and bottom interfaces + bulk) and assuming that the bulk charge carriers are three-dimensional (3D), we used the available literature data on the parameters of the electron spectra to estimate the electron densities corresponding to each group. Thus, we were able to divide the total charge carrier density into the surface and bulk contributions. In this simple approach, for the interface carriers we have obtained concentration values of about  $5 \times 10^{12} \text{ cm}^{-2}$ , which are physically more suitable, although, still relatively high. As for the bulk carriers,

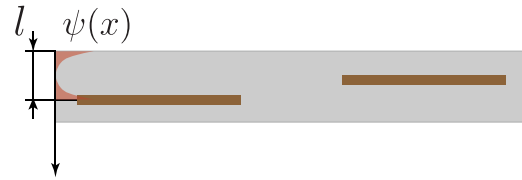


**Figure 4.** Schematic layout used in the estimations of magnetic interactions in a film with inclusions.

obtained concentration values ( $(1-3) \times 10^{19} \text{ cm}^{-3}$ ) are close to that of ordinary 3D  $\text{Bi}_2\text{Se}_3$  crystals, but the corresponding Fermi momenta are also relatively high, which will be used in the next section.

## 4. Theoretical analysis

### 4.1. Basic picture

Here, we outline the theoretical considerations with the aim to clarify the physical mechanisms underlying the ferromagnetic ordering in the films under study. Note that usually, if we have magnetic impurities in a material with itinerant charge carriers, these charge carriers mediate indirect exchange interaction (IEI) of the RKKY type between impurities. In our films containing flat magnetic inclusions, the situation is more complicated and intriguing. Indeed, there exist several possible mechanisms of the magnetic interaction, let us list the most important ones:

- (i) Heisenberg-type direct exchange and superexchange,
- (ii) IEI via charge carries at the surface of the topological insulator,
- (iii) IEI via charge carries in the bulk,
- (iv) magnetic dipole–dipole interactions (MDD).

The Heisenberg-type exchange interactions (i) can be relevant only at short distances of the order of lattice constant (mainly inside magnetic platelets). Interactions (ii) and (iii) are of the RKKY-type (interaction via itinerant charge carriers) and differ only by the spectra of charge carriers and by the spatial regions where the carriers are present. Normally, the dipole–dipole interaction (iv) in the systems with magnetic impurities is rather weak, when one calculates the corresponding contribution of magnetic moments for isolated atoms. In our case, however, we consider relatively large magnetic objects, namely Eu-rich flat magnetic inclusions, which contain  $\sim 10^3$  Eu atoms with the mean size of inclusions up to 15–20 nm (the thickness of isolated inclusion is less than 1 nm). Hence, it is natural to expect that the MDD interactions could be relevant here.

Although we have not been yet able to determine the specific form of inclusions, the absence of the pronounced crystallographic anisotropy of transport properties in the film plane suggests that the sizes of an inclusion along any given in-plane direction should not differ much.

Now, let us perform some estimates for each of these types of interaction. Probably, the easiest estimate is that for the RKKY interaction via the surface charge carriers. The crucial

observation is that the electrons of the surface and electrons of the inclusion are always separated by the minimum distance  $l$ , being the depth of inclusion location below the surface (see figure 4). As a result, the corresponding exchange integral entering the strength of the interaction is exponentially suppressed

$$J_{\text{surface}} \sim J_0 e^{-l/l_0}, \quad (1)$$

where  $l_0$  is the characteristic scale of the wave function and  $J_0$  is the exchange constant in the bulk. Thus, for studied films, this type of interaction appears to be irrelevant.

In the following subsections, we present less trivial estimates. Below, we use following notation (denoting magnetic  $\text{Eu}^{2+}$  ions simply as Eu atoms):  $L_0$  is the characteristic size of inclusions,  $N_0$  is the total volume concentration of Eu,  $N_i$  is the total volume concentration of inclusions,  $R_0$  is the characteristic distance between inclusions,  $d_0$  is the distance between Eu atoms inside an inclusion, and  $N_p$  is the average number of Eu atoms in an inclusion.

#### 4.2. Magnetic interactions within inclusions

The initial step is the estimate of the magneto-dipole interaction inside an inclusion, which can be written in a simple form

$$E_{\text{MDD}} = \frac{\mu_0 \mu_B^2 [7/2]^2}{d_0^3}, \quad (2)$$

where  $\mu_B = e\hbar/2m_e$  is the Bohr magneton. First, we need to estimate the average distance  $d_0$  between impurities in an inclusion. Obviously, distances between Eu atoms depend on an actual crystal structure of an inclusion. Unfortunately, we have no exact data on the atomic structure of the inclusion itself, but we suppose that it should be close either to EuSe or to  $\text{Bi}_2\text{Se}_3$ . Due to high Eu content within an inclusion ( $\sim 1000$  atoms per platelet), we suppose that  $d_0$  values are of the order of corresponding lattice constant  $a \approx 6.5 \text{ \AA}$  (arithmetic mean for EuSe and  $\text{Bi}_2\text{Se}_3$  lattice constants). Thus, we have an estimate for MDD contribution

$$E_{\text{MDD}} \approx 0.4 \text{ K}. \quad (3)$$

Let us now estimate the characteristic energy of the RKKY interaction. The corresponding formula is presented in [18]:

$$E_{\text{RKKY}} \sim \left[ J_1^2 \frac{E_F^2 m_{\text{eff}}^3 d_0^3}{\hbar^6 (k_F)^3} \right] \cos(2k_F d_0), \quad (4)$$

where  $J_1$  is the exchange coupling between the magnetic moment of an Eu atom and of a conduction electron (measured in Kelvin),  $m_{\text{eff}}$  is the effective mass of itinerant charge carriers and  $k_F$  is the Fermi momentum. Here, we need to make an important remark. The strong spin-orbit coupling in  $\text{Bi}_2\text{Se}_3$  [2] leads to the more general type of spin structure of RKKY interaction. Its spin part in general, have a form [19]  $\alpha \mathbf{S}_1 \mathbf{S}_2 + \beta (\mathbf{S}_1 \mathbf{n})(\mathbf{S}_2 \mathbf{n})$  where  $\mathbf{S}_{1,2}$  are Eu spins,  $\mathbf{n}$  is the unit vector connecting their positions and  $\alpha, \beta$  are coefficients of the order of unity. It is not necessarily FM *a priori*.

However, as it was mentioned earlier, low-temperature nonlinear magnetic response of studied films and distinct

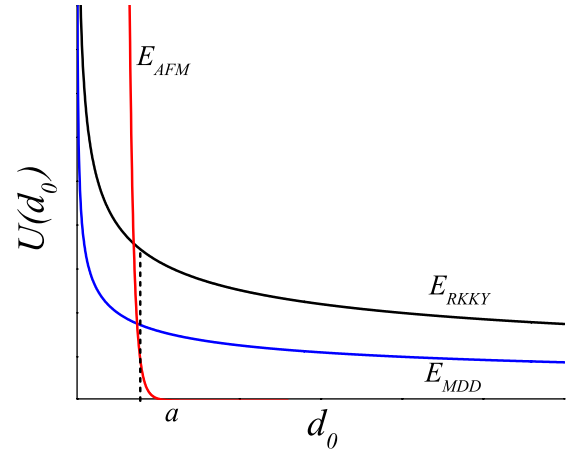


**Figure 5.** Schematic picture of interactions inside the inclusion: the strength of different interaction mechanisms as a function of distances between Eu atoms.  $a$  is the lattice constant.

hysteresis loop observed for  $x = 0.21$  sample (see figure 3) suggests that inclusions themselves are ferromagnetically ordered. Therefore, we use the simplest  $\mathbf{S}_1 \mathbf{S}_2$  FM form of RKKY.

Taking the estimated value of bulk Fermi energy  $E_F \approx 150 \text{ meV}$  (for a sample with  $x = 0.038$ , see appendix A.2) and the effective mass  $m_{\text{eff}} \approx 0.13m_e$  [20], we arrive at

$$E_{\text{RKKY}} \sim 6 \times 10^{-6} \text{ K}^{-1} J_1^2. \quad (5)$$

Here, we put  $\cos(2k_F d_0) \approx 1$  taking into account that  $2k_F d_0 \approx 1$ . Finally, the typical order of magnitude for the exchange integral between the band electrons and localized magnetic moment of Eu is of the order of tenths of an eV (see e.g. [21, 22])

$$J_1 \approx 0.2 \text{ eV} \approx 2300 \text{ K}. \quad (6)$$

Therefore, the scale of RKKY interaction is

$$E_{\text{RKKY}} \sim 30 \text{ K}. \quad (7)$$

As it was described above, the structure of inclusions in the studied films may be close to that of EuSe compound, meaning that magnetic properties of these systems can be similar. The exchange interaction via cation electrons in EuSe have been studied earlier [23–25] and revealed the presence of considerable antiferromagnetic (AFM) contribution which decreases with the distance according to Grueneisen law  $\sim 1/d_0^{12.2}$ . Being interested only in the order of magnitude estimates, we assume that inclusions have the EuSe lattice stretched by Bi. Thus, we can estimate the AFM contribution in our case as

$$E_{\text{AFM}} \sim 0.2 \text{ K}. \quad (8)$$

To compare different contributions into overall exchange interaction in the studied films, one can plot a simple scheme presented in figure 5. The AFM contribution is severely reduced at distances larger than lattice constant  $a$  (if we apply results for EuSe compound), which suggests that in studied films  $d_0 > a$ , because the overall exchange in this case should provide FM ordering, which agrees with the experiment. Thus, within platelet inclusions, the FM state is established mainly via the RKKY interaction.

It is important to mention that magnetic moments within inclusions will be oriented in-plane. Thus, to reorient moments out-of-plane an external field should be applied. Simple estimation of the reorientation field ( $E_{\text{RKKY}} \sim (7/2)\mu_B H_\perp$ ) for  $E_{\text{RKKY}} \sim 30\text{ K}$  gives  $H_\perp \sim 13.5\text{ T}$ . The actual value of reorientation field for the whole sample may be different if one apply more accurate estimation procedure and take into account long-range interactions (i.e. between platelets, see below), but it will be of order of at least several Tesla. The latter suggests that magnetotransport anisotropy of studied films in low field region is not affected by in-plane to out-of-plane reorientation of magnetic moments [16], although anisotropy at higher magnetic field should be treated more carefully.

#### 4.3. Interactions between inclusions

We start with the in-plane interaction, meaning that we consider the case when interacting magnetic moments and platelet inclusions themselves lie in one plane. As will be argued below, this planar approximation is justified for small concentrations of Eu. As in the case of inner-platelet, the RKKY interaction at large distances has quite general spin structure (due to the strong spin-orbit coupling in  $\text{Bi}_2\text{Se}_3$ ) and can be written as (see equation (5))

$$E_{\text{RKKY}}^{\text{inter}} = 6 \times 10^{-6} K^{-1} J_1^2 \left( \frac{d_0}{r} \right)^3 \times \cos 2k_F r f_{\text{spin}}(\mathbf{s}_1, \mathbf{s}_2), \quad (9)$$

where the  $f_{\text{spin}}$  is some spin function. Taking into account (4) and (5), we write down the following integral for the RKKY interaction between two platelets

$$E_{\text{RKKY}}^{\text{inter}} = 6 \times 10^{-6} K^{-1} J_1^2 \left( \frac{N_p}{\pi L_0^2} \right)^2 \times \int_{\text{platelets}} \left( \frac{d_0}{|\mathbf{r} - \mathbf{r}'|} \right)^3 \cos 2k_F |\mathbf{r} - \mathbf{r}'| d\mathbf{r} d\mathbf{r}' f_{\text{spin}}(\mathbf{s}_1, \mathbf{s}_2). \quad (10)$$

The integral is estimated in appendix A.2. Here, we should mention the following thing. The principal distinctive feature of the RKKY interaction is its oscillatory behavior on the scale of  $1/k_F$ . Therefore, the interaction changes its sign many times on the scale of the size of the platelet  $L_0 \gg 1/k_F$ . This results in the suppression of the integral interaction by the cubic power of  $k_F L_0$ . The resultant interaction can be written as

$$E_{\text{RKKY}}^{\text{inter}} = 6 \times 10^{-6} K^{-1} J_1^2 N_p^2 \left( \frac{d_0}{R} \right)^3 \times \frac{1}{(k_F L_0)^3} \cos 2k_F R \cos^2(k_F L_0 - 3\pi/4) f_{\text{spin}}(\mathbf{s}_1, \mathbf{s}_2), \quad (11)$$

(see appendix A.2 for details). We would like to compare this interaction with the magneto-dipole interaction between the platelets. Unlike the RKKY interaction, the magneto-dipole interaction between the inclusions does not oscillate with

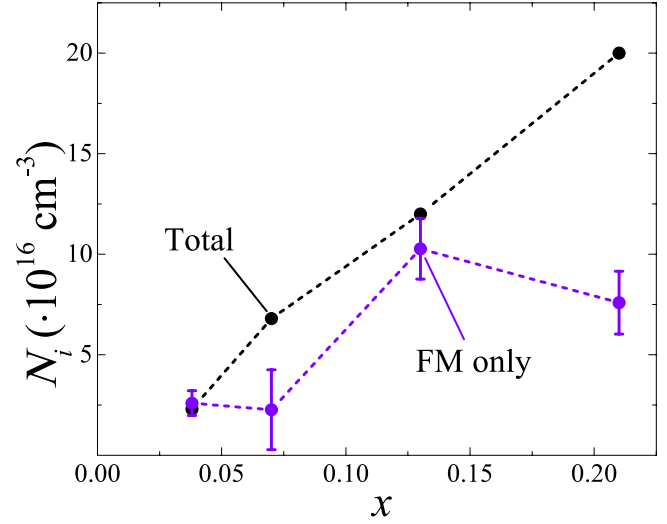


**Figure 6.** AFM stacking: dependence of the concentration of inclusions on Eu content—total concentration and concentration of FM inclusion only (accounting for the AFM stacking).

the distance. Therefore, it can be estimated as an interaction between point-like magnetic moments

$$E_{\text{MDD}}^{\text{inter}} = E_{\text{MDD}} N_p^2 \left( \frac{d_0}{R} \right)^3 [\mathbf{s}_1 \mathbf{s}_2 - 3(\mathbf{s}_1 \mathbf{n})(\mathbf{s}_1 \mathbf{n})]. \quad (12)$$

Finally, we see that the relative strengths of upper bound of the RKKY interaction between inclusions and the magneto-dipole interaction are

$$E_{\text{RKKY}}^{\text{inter}} \sim 6 \times 10^{-6} J_1^2 \frac{1}{(k_F L_0)^3} E_{\text{MDD}}^{\text{inter}} \approx 0.1 E_{\text{MDD}}^{\text{inter}} < E_{\text{MDD}}^{\text{inter}}. \quad (13)$$

Hence, we come to the conclusion that the magneto-dipole contribution is the dominant one in the interaction between inclusions for all relevant  $R$  values.

#### 4.4. Stacking of inclusions

Now let us consider a case of two interacting inclusions located one under another at distance  $t$  (i.e. forming a stack). Due to apparent anisotropy of a single platelet the corresponding magnetic moment should be oriented within its plane. Thus, we deal with two parallel moments, which for the magneto-dipole interaction usually leads to a AFM ordering. Indeed, such inclusion placement results in strong AFM bonding with  $J_{\text{stack}} \sim 100\text{ K}$ . Hence, the magnetic field required for their reorientation is way above 10 kOe. It explains the decrease in the average magnetic moment per Eu atom,  $\mu_{\text{Eu}}$ , at higher  $x$  values observed in experiment. Suggesting that such AFM stacking is the main cause of decrease in the  $\mu_{\text{Eu}}$ , one can estimate the concentration of only FM platelets (see figure 6). It can be seen that concentration of FM platelets increases slower than overall inclusion concentration  $N_i$

$$\frac{7}{2} \mu_B (N_i - N_{\text{AFM}}) = \mu_{\text{Eu}} N_i. \quad (14)$$



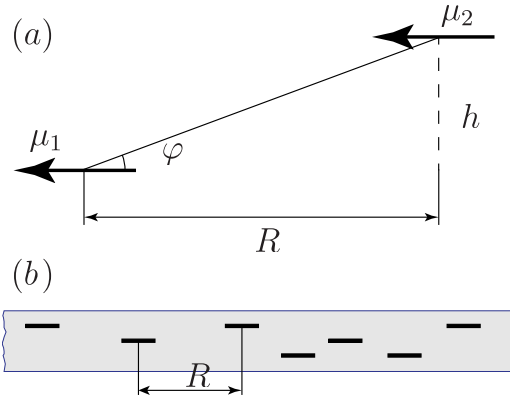


**Figure 7.** Schematic illustration of the interaction between magnetic inclusions: (a) mutual positions of magnetic moments belonging to neighboring platelets; (b) distribution of platelets within the film.  $R$  is the average planar distance between platelets.

Here, we denoted by  $N_{\text{AFM}}$  the number of AFM ordered platelets due to stacking. In case of stacks of platelets, the RKKY interaction is much more difficult to estimate since the distance between the inclusions is  $R \ll L_0$  for some portions of the inclusions. Yet we understand that in comparison to the magneto-dipole interaction (for which a reliable estimate can be made, see below), the RKKY interaction will have the additional fast oscillating cosine factor as one moves from one Eu atom to another, and it will again be suppressed as compared to the nonoscillating magneto-dipole interaction.

Considering a system with magnetic platelet inclusions, that can form AFM stacks when Eu content is large enough, it is important to account for finite thickness of the film. Basically, it means that overall interaction between two platelets can result in the AFM ordering not only when platelets are located one under another (i.e. forming a stack), but also at some critical angle  $\varphi$  between moments of platelet pair (see figure 7(a)). It is obvious that maximum angle between moments of a pair, in average, depends solely on the film thickness (assuming that platelets are distributed randomly). Let us recall a simple estimate of the width of the material, at which ferromagnetic interaction between dipoles is turned into the antiferromagnetic one.

Thus, the dipole–dipole interaction energy should vanish at some angle  $\varphi$

$$E = \mu_1 \mu_2 \frac{1 - 3 \cos^2 \varphi}{r^3} = 0, \quad (15)$$

thus, we obtain

$$\cos \varphi = \frac{1}{\sqrt{3}}, \quad h = \sqrt{2}R, \quad (16)$$

where  $R$  and  $h$  are the planar and vertical distance between inclusions respectively. For lowest concentration of Eu the average magnetic moment is largest suggesting that there are almost no stacks of inclusions. Therefore, the inclusions have purely planar distribution (as in figure 7(b)), so we can neglect vertical displacements between platelets. This means that the average planar distance between the inclusions can be estimated as

$$R \approx 1/\sqrt{N_i d} = N_{\square}^{-1/2}. \quad (17)$$

The thickness of the sample with  $x = 0.07$  is  $d \approx 26$  nm and the concentration of inclusions is  $N_i \approx 7 \times 10^{16} \text{ cm}^{-3}$ . Hence, the film will contain  $N_{\square} \approx 0.18 \times 10^{12}$  inclusions per  $\text{cm}^2$ . This implies the average planar distance between impurities  $\approx 23$  nm. Thus, the characteristic vertical distance between inclusions, at which the ferromagnetic interaction can change to antiferromagnetic one, is therefore,  $h \approx 33$  nm. This is larger than the actual thickness of our typical sample, the difference is even more pronounced at lower  $x$ . Therefore, we can, at least, qualitatively consider all the inclusions to be coplanar.

It is worth mentioning that a more detailed estimation of platelet interaction within a stack can be performed (see appendix A.3). Within such approach we consider interaction of two parallel platelets with a small spacing between them (corresponding to several quintlayers of  $\text{Bi}_2\text{Se}_3$ ) as a function of relative horizontal position. It appears, that platelets remain AFM ordered until they have overlapping region of at least 0.2–0.3 of the platelet area. On the one hand, it implies that AFM stacking do not require a fixed platelet location (platelet centers in a stack can be substantially shifted). On the other hand, small overlapping (e.g. overlapping edges of platelets) does not lead to the AFM ordering. Based on the estimations made, we do not have to account for the intermediate states. Basically, we can limit ourselves to a simple model, where the AFM stacking affects only the overall magnetic moment of the system, whereas the interaction at larger distances does not include a significant AFM contribution (due to the small film thickness).

#### 4.5. Theoretical estimate for the transition temperature

In previous subsections, we were dealing with pair interactions, now we will consider the whole ensemble of platelet inclusions. To perform theoretical estimates, we employ the technique developed in [26, 27] for metallic spin glasses. We model our system by a classical disordered Heisenberg chain model, assuming Eu-rich platelets as point-like magnetic centers. The Hamiltonian takes into account the fact that the magnetic centers are located at some sites of the effective lattice and not at all of them

$$H(s) = -\frac{1}{2} \sum_{\mathbf{r}, \mathbf{r}'} J(\mathbf{r} - \mathbf{r}') s_{\mathbf{r}} s_{\mathbf{r}'} c_{\mathbf{r}} c_{\mathbf{r}'} - H \sum_{\mathbf{r}} s_{\mathbf{r}} c_{\mathbf{r}},$$

where  $s_{\mathbf{r}}$  denotes the spin at site  $\mathbf{r}$  and  $c_{\mathbf{r}} = 0$  or 1 depending on whether a spin occupies site  $\mathbf{r}$  or not.  $J(\mathbf{r} - \mathbf{r}')$  is the interaction between sites  $\mathbf{r}$  and  $\mathbf{r}'$ .

This random site problem (the randomness comes from the distribution of spins in a lattice) can be solved in the low-concentration limit via a mean-field approximation in the replica scheme. In [27] it is argued that at small concentration of magnetic impurities, the system undergoes the transition into

a spin-glass state at the critical temperature determined by the following equation

$$N_{\square} = \sum_{\mathbf{r}} \tanh^2[\beta J(\mathbf{r})] = 1,$$

where  $N_{\square}$  models the 2D density of inclusions and the summation is taken over the lattice sites  $\mathbf{r}$ .

Therefore, the switching from summation to integration, we arrive at the following equation

$$\frac{\pi}{R^2} \int_0^{\Lambda} dr r \tanh^2 \left[ \frac{E_{\text{MDD}} N_p^2}{T_c} \left( \frac{d_0}{r} \right)^3 \right] = 1. \quad (18)$$

Here, the interaction cutoff  $\Lambda$  should be taken to be equal to infinity, since the magneto-dipole interaction has no screening length.

For  $x = 0.038$ , the characteristic distance between the inclusions is  $R \approx 42$  nm (in accordance with (17)). Note here, that due to the lack of inclusion stacking for small concentrations of Eu, we model our system as an effectively two-dimensional one (see the previous subsection).

In general, the integral can be expressed via the Riemann zeta function, but here, it is sufficient to make a simple estimate

$$\frac{2\pi d_0^2}{R^2} \left( \frac{E_{\text{MDD}} N_p^2}{T_c} \right)^{2/3} 0.65 \approx 1. \quad (19)$$

Finally, we arrive at the following expression for the critical temperature

$$T_c \approx (2\pi)^{3/2} \left( \frac{d_0}{R} \right)^3 E_{\text{MDD}} N_p^2. \quad (20)$$

Thus, for  $x = 0.038$  sample, we obtain  $T_c \approx 3.5$  K, which is relatively close to experimental value (see section 4.6).

As we have mentioned above, the increase in  $N_0$  leads to almost linear growth of  $N_i$  (see figure 6), which implies that the number of Eu atoms per inclusion  $N_p = N_i/N_0$  remains approximately the same. Thus, reproducing the dependence of  $R$  on  $N_i$  for thin films, we eventually arrive at the following relation for the critical temperature

$$T_c \propto N_i^{2/3}. \quad (21)$$

Relation (21) is the main result of the theoretical discussion. It is important to note, that assumptions of point-like inclusions having fixed magnetic moments ( $\sim N_p$ ) at various Eu concentrations corresponds to the original result for the metallic spin glasses obtained in [26]. In original model, the power of 2/3 is ascribed to the presence of non-magnetic impurities, while for pure metals the power is 1/3 [26]. However, in our case, we consider the MDD interaction (not RKKY), for which no other powers are expected, while power 2/3 arise from the fact that we consider our system as effectively a 2D one. Thus, we assume that relation (21) does not depend on the other details of a system.

#### 4.6. Discussion

Let us now summarize the obtained results. Initially, experimentally observed weak dependence of the nonlinear response to the applied magnetic field on the Eu doping, alongside with the decreasing magnetic moment per Eu atom, suggested a complicated character of the evolution of the properties of the magnetic subsystem with the increase in  $x$ . To describe experimental data, we have estimated the role of various interaction mechanisms providing the contributions at two scales—inside the platelet inclusions and between them.

While studied films preserve the same morphology at various Eu content (inclusions have the platelet-like shape), the presence of a distinct hysteresis loop at higher  $x$  values suggests that magnetic moments of Eu atoms in a single platelet are ferromagnetically ordered. Our estimations suggest that inside a platelet, the dominant contributions can be attributed to the RKKY mechanism yielding the ordering temperature values of about 30–40 K, which agrees with the experiment. Note, however, that we are not yet able to formulate a full theory of magnetic physics inside the inclusion since its atomic structure is not known in detail. Indeed, the underlying physics depends on such structure in an essential way. For example, if the inclusion corresponds to a state under high pressure (exerted by the parental  $\text{Bi}_2\text{Se}_3$  compound), then the interaction inside the inclusion is determined by an interplay between antiferromagnetic exchange interaction and FM and AFM parts of the RKKY interaction. It demands for further structural studies.

To obtain saturation of magnetization at fields below 1 T at temperatures 10–20 K, the platelet inclusions have to be interacting. Our analysis shows that, due to large number of Eu atoms within a platelet, the dominant contribution stems from the MDD interaction, whereas the fast-oscillating RKKY contribution is damped at large distances. When two platelets form a stack (located one under another), the MDD interaction leads to a strong AFM coupling. We argue that AFM stacking does not affect the in-plane interactions in sufficiently thin films. Thus, we conclude that AFM stacking is responsible only for the decrease of magnetic moment  $\mu_{\text{Eu}}$  per Eu atom at higher  $x$ , suggesting that the number of platelets interacting at large distances can be substantially smaller than overall concentration of inclusions  $N_i$ .

At small  $x$  values, when the distances between inclusion centers are much larger than their size, it is possible to consider the system as a dilute magnetic semiconductor. In this case, we employ the theory developed earlier for such compounds [26, 27] and estimate the critical temperature, at which the ensemble of magnetic inclusions undergoes the spin-glass ordering. It is worth mentioning that the MDD interaction of randomly distributed magnetic centers can, in principle, lead not only to the spin-glass state but also to chiral order (if some additional conditions are met). In our case, the spin glass structure explains the absence of a pronounced hysteresis at small concentrations of Eu, while at higher  $x$  values

such theory becomes inapplicable and we cannot use it as a relevant model.

It is important to note that obtained value of  $T_c \approx 3.5$  K for  $x = 0.038$  appears to be rather small. However, this estimation was made for zero field limit, while experimental values of 8–15 K were obtained in magnetic field, thus, some difference in values was anticipated. Nevertheless, we can use relation (21) for another rough estimation. If the AFM stacking phenomena is taken into account, one can see that the increase of  $N_i$  by a factor of nine at higher  $x$  results only in a four times higher concentration of platelets interacting at large distances. Thus, relation (21) suggests that  $T_c$  should increase only by a factor of 2.5, which is roughly coincides with the experimental uncertainty in the determination of  $T_c$ .

Thus, we have formulated a qualitative model of the magnetic subsystem in the films under study, which explains the main observed experimental features.

## 5. Conclusions

In this paper, we have formulated a semiquantitative theoretical interpretation of interaction between magnetic impurities in  $\text{Bi}_2\text{Se}_3$  doped by Eu. The experimental observation shows that Eu atoms have an extremely inhomogeneous distribution, namely, they form platelet-like nanoinclusions, which become ferromagnetic at low temperatures. Due to relatively large thickness of studied films the overall contribution of RKKY interaction via interface Dirac electrons is damped by a factor of  $e^{-l}$ , with  $l$  being the vertical distance between inclusion and the film interface. It allows us to attribute the observed magnetic phenomena solely to the bulk properties, which makes a basis for the consideration of thinner films with analogous magnetic phase profile.

The estimated Fermi energies of the bulk charge carriers are high enough to impart a fast-oscillating character of the RKKY interaction, which still allows the corresponding contribution to dominate at small distances (i.e. within platelets) yielding FM ordering, but makes it too small on the inter-platelet scale. Considering Eu-rich platelets as a superspin particles (with more than 1000 Eu atoms per inclusion) it becomes evident that leading contribution at large distances is related to the magnetic dipole–dipole interaction. Thus, the formation of the ferromagnetically correlated state that explains the magnetization saturation at low fields, is governed by the MDD interaction, which also underlies the decrease in the average magnetic moment per Eu atom. The latter is related to the AFM ordering of stacks of platelets, which presence is confirmed experimentally, suggesting that concentration of platelets interacting at larger distances is substantially smaller at high Eu content than that implied by the overall concentration of inclusions. As we take into account a finite film thickness, it turns out that the studied systems can be treated as effectively 2D, yielding only one sign of the MDD interaction if the AFM stacking phenomena are involved.

Thus, we have employed the model of the disordered metallic spin glass and found out the characteristic concentration dependence for the transition temperature (21),

neglecting the effects of anisotropy of the considered system. The randomness of platelet spatial distribution combined with MDD interaction makes the aforementioned correlated state of spin glass character, which confirms the applicability of the used model and explains the absence of pronounced hysteresis loop at low Eu content, where this model can be considered as a rigorous one. The qualitative estimate of transition temperature  $T_c$  yields a satisfactory numerical agreement with the experimental results, moreover, taking the AFM stacking into account shows that range of  $T_c$  changes upon the increase of Eu content falls within experimental uncertainty region. These results strengthen our confidence that the underlying assumptions of our derivations are correct.

It is worth mentioning that studied distribution profile for the magnetic subsystem is quite promising for the realization in ultrathin films. While the MDD interaction of randomly distributed platelets is lacking of rigid collinear ordering within sample plane, it paves way for an effective impact of external factors, for example, of Dirac electrons at the interfaces. This contribution should be sufficiently larger for ultrathin films compared to our case. Considering the nontrivial spin structure of Dirac electrons, in principle, it is possible to engineer chiral spin structures either of platelet itself, or of the platelet ensemble by changing sizes and spacings between inclusions.

## Acknowledgments

The work was partially supported by the Russian Science Foundation, grant No. 17-12-01345. We are grateful to the Resource Center of NRC ‘Kurchatov Institute’ for use of the available equipment and for helpful assistance.

## Appendix

### A.1. Estimate of the Fermi energy

Here, we compute the Fermi energy of electrons in the bulk. The total charge carrier concentration  $N_{\text{Hall}}$  was deduced from Hall measurements (representing electron density per square of the film). We model our films as a vessel of three groups of charge carriers (see figure A1)—two interfaces and bulk. Constant Fermi level implies that Fermi energies for the interface and bulk charge carriers differ by the  $E^{\text{Dir}}$  value. Considering the interface charge carriers as Dirac electrons with  $E = \hbar v_F |k|$  spectrum, we can use following equation

$$N_{\text{Hall}} = N_{\text{vol}}(E_{\text{F}}^{\text{vol}})d + 2 \frac{(E_{\text{F}}^{\text{vol}} + E^{\text{Dir}})^2}{4\pi v_{\text{F}}^2 \hbar^2}. \quad (\text{A.1})$$

The spectrum of bulk  $\text{Bi}_2\text{Se}_3$  corresponds to ellipsoidal Fermi surface with  $E_{\text{F}}$ -dependent anisotropy. To obtain  $E_{\text{F}}$  values, we apply the relations used for the determination of electron density in bulk  $\text{Bi}_2\text{Se}_3$  crystals from the Shubnikov–de Haas measurements [28–30]. Rewriting relevant relations, we arrive at

$$E_{\text{F}} = \frac{\pi \hbar^2}{2m_{\text{eff}}} \left( \frac{9\pi N_{\text{vol}}^2}{\eta^2} \right)^{1/3}, \quad (\text{A.2})$$

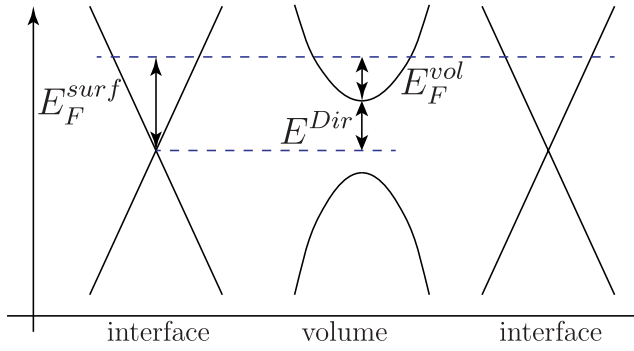


**Figure A1.** Schematic picture for spectrum and Fermi levels of bulk and surface electrons.

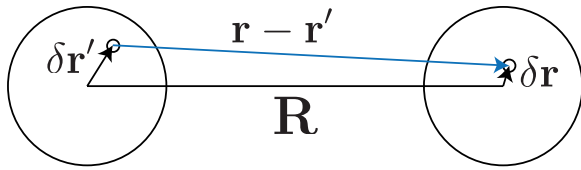


**Figure A2.** Computation of the interplatelet interaction.

where  $\eta$  is the anisotropy factor. Usually  $\eta \in [1, 2]$  and increases linearly with the oscillation frequency (proportional to Fermi energy) [28]. For simplicity, we used ordinary power-law formula with  $\eta \sim N_{\text{vol}}^{2/3}$  for interpolation of reference data and combined it with (A.2). For the interface charge carriers, we used values  $E^{\text{Dir}} = 0.3$  eV and  $v_F = 5 \times 10^5$  m s $^{-1}$  from [31]. It is worth mentioning that within this estimation, to obtain values of electron densities determined experimentally for pure Bi $_2$ Se $_3$  films reported previously (see [32]), one needs to tune parameters of estimation. For example, changing the Fermi velocity to  $v_F = 8.55 \times 10^5$  m s $^{-1}$  gives a good agreement with experimental values and lower densities for interface carriers (which is physically more suitable). Nevertheless, the discrepancy of  $E_F$  values for Eu-doped samples at different  $v_F$  are below 15%, thus we consider it rather trustworthy.

As it was mentioned in the main text, described estimation gives for sample with  $x = 0.038$  and  $N_{\text{Hall}} = 6.2 \times 10^{13}$  cm $^{-2}$  the value  $E_F \approx 150$  meV.

### A.2. Calculation of the interplatelet interactions

Let  $\mathbf{R}$  be the vector connecting the centers (see figure A2),  $\mathbf{n} = \mathbf{R}/R$ . Let us also assume that the inclusions are well separated, meaning that the average distance between platelets is much larger than their size,  $L_0 \ll R$  (in fact, in our case, we have  $L_0 \lesssim R$ , but for a simple estimate, it is acceptable to change  $\lesssim \leftrightarrow \ll$ ). Then,  $|\mathbf{r} - \mathbf{r}'| \approx R + \delta\mathbf{r} \cdot \mathbf{n} - \delta\mathbf{r}' \cdot \mathbf{n}$ . Next, we perform the integration introducing dimensionless vectors  $\mathbf{s} = \delta\mathbf{r}/L_0$ ,  $\mathbf{s}' = \delta\mathbf{r}'/L_0$ . In fact,  $k_F L_0 \approx 5$  can be considered as a large parameter. We use the standard integral representation for the Bessel function. As a result, we have

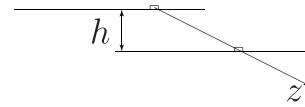
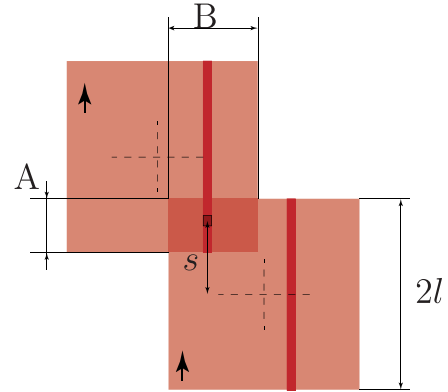
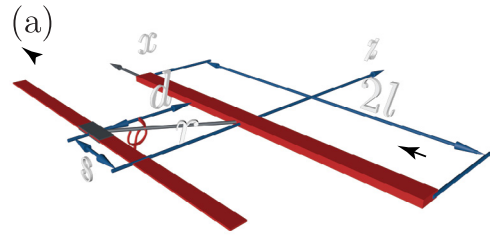


**Figure A3.** Layout illustrating the interaction between magnetic platelets.

$$\begin{aligned} & \int d\varphi d\varphi' d\mathbf{r} d\mathbf{r}' \cos(2k_F |\mathbf{r} - \mathbf{r}'|) = L^4 \cos(2k_F R) \\ & \times \left[ 2\pi \int_0^1 J_0(2k_F L_0 s) s ds \right]^2 = \left( \frac{\pi L^2}{k_F L_0} \right)^2 [J_1(2k_F L_0)]^2 \\ & \times \cos(2k_F R) \approx (\pi L^2)^2 \frac{\cos(2k_F R)}{\pi (k_F L_0)^3} \cos^2 \left( 2k_F L - \frac{3\pi}{4} \right), \end{aligned} \quad (\text{A.3})$$

$k_F L_0 \gg 1$ .

Using this expression, we immediately recover formula (11) in the main text.

### A.3. Estimate of the finite dipole–dipole interactions

For a qualitative estimate, it is sufficient to compute the interaction energy between two square platelets with the aligned magnetic moments. Let us first consider the interaction of two shifted dipole lines of length  $2l$  each (see figure A3). The shift length is  $2l - \Delta$ . The field of magnetic dipole

$$dB_x = \frac{\mu}{2l} \frac{3 \sin^2 \varphi - 1}{d^2} \cos \varphi d\varphi dB_z = \frac{\mu \cos^2 \varphi \sin \varphi}{2l} \frac{d\varphi}{d^2}. \quad (\text{A.4})$$

Note that the  $z$  axis is in fact tilted.

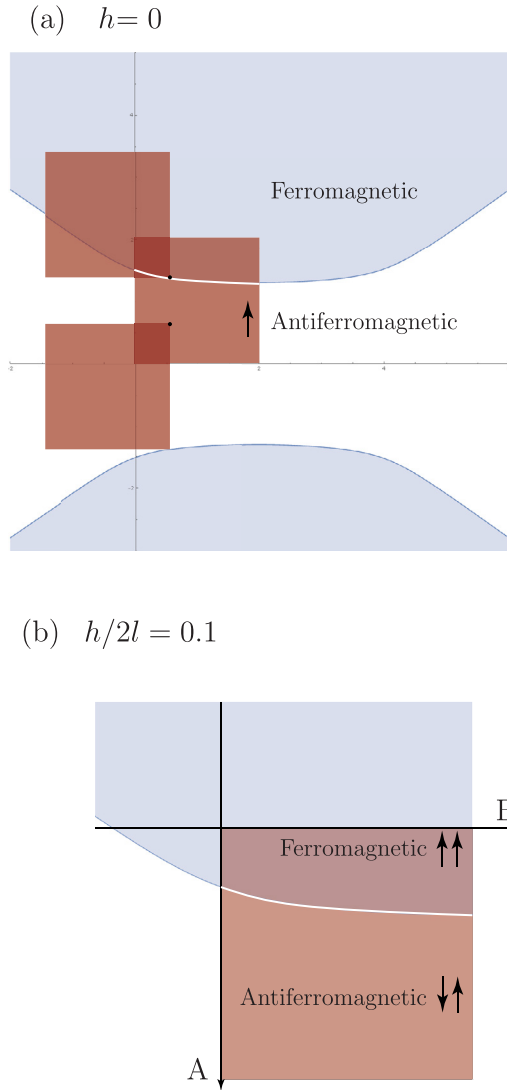


**Figure A4.** Critical overlay curve (white) for the crossover between the FM and AFM alignment of the magnetic moments of platelets. (a)  $h = 0$ , (b)  $h/2l = 0.1$ .

As a result, the full magnetic field is

$$B_x(s) = \frac{\mu}{2ld^2} \left( \frac{(l-s)^3}{[(l-s)^2 + d^2]^{3/2}} + \frac{(l+s)^3}{[(l+s)^2 + d^2]^{3/2}} - \frac{(l-s)}{[(l-s)^2 + d^2]^{1/2}} - \frac{(l+s)}{[(l+s)^2 + d^2]^{1/2}} \right)$$

$$B_z(s) = -\frac{\mu}{d2l} \left( \frac{1}{[(l-s)^2 + d^2]^{1/2}} - \frac{1}{[(l+s)^2 + d^2]^{1/2}} \right).$$

The full interaction between two platelets (depicted as lines) have the form

$$dE_{\text{lines}} = - \int_{l-A}^{3l-A} B_x(s) \frac{\mu}{2l} ds = -\frac{\mu^2}{2l^2} \left( \frac{1}{[A^2 + d^2]^{1/2}} + \frac{1}{[(A-4l)^2 + d^2]^{1/2}} - \frac{2}{[(A-2l)^2 + d^2]^{1/2}} \right).$$

Finally, we have  $d^2 = h^2 + (y_1 - y_2)^2$ , and the full interaction energy between two square platelets reads:

$$E_{\text{full}} = \int_{-2l+B}^B dy_2 \int_0^{2l} dy_1 dE_{\text{lines}}$$

$$E_{\text{full}} = F(A, B) + F(A - 4l, B) - 2F(A - 2l, B),$$

$$F(\Delta, B) = B \operatorname{arcsinh} \frac{B}{\sqrt{\Delta^2 + h^2}} - (2l - B) \times \operatorname{arcsinh} \frac{2l - B}{\sqrt{\Delta^2 + h^2}} + \sqrt{(2l - B)^2 + \Delta^2 + h^2} - \sqrt{B^2 + \Delta^2 + h^2}.$$

Now, we can compute the FM curve  $A(B)$ , namely, the curve where the potential energy of parallel moments is zero. This function can be found numerically. Let us consider two cases:  $h/2l = 0$  (almost touching overlaying platelets) and  $h/(2l) = 0.2$  (typical of the experiment). Then, we present the corresponding plot in figures A4(a) and (b). We see that the critical FM–AFM overlay curve: (i) does not change qualitatively as we change the respective overlay height from  $h = 0$  to  $h = 0.1$ ; (ii) is not very different from the line and gives the critical overlay percentage of the area of platelets to be  $x \in [0.25, 0.33]$ . The estimate should remain qualitatively the same for the platelets of any geometry.

### ORCID iDs

L N Oveshnikov  <https://orcid.org/0000-0003-1950-4607>

### References

- [1] Fu L and Kane C L 2007 *Phys. Rev. B* **76** 045302
- [2] Hasan M Z and Kane C L 2010 *Rev. Mod. Phys.* **82** 3045
- [3] Qi X-L and Zhang S-C 2011 *Rev. Mod. Phys.* **83** 1057
- [4] Liu C-X, Zhang S-C and Qi X-L 2016 *Ann. Rev. Condens. Matter Phys.* **7** 301
- [5] Lu H-Z, Shi J J and Shen S-Q 2011 *Phys. Rev. Lett.* **107** 076801
- [6] Liu M *et al* 2012 *Phys. Rev. Lett.* **108** 036805
- [7] Yang Q I *et al* 2013 *Phys. Rev. B* **88** 081407
- [8] Fan Y *et al* 2016 *Nat. Nanotechnol.* **11** 352
- [9] Liu C, Zang Y, Ruan W, Gong Y, He K, Ma X, Xue Q-K and Wang Y 2017 *Phys. Rev. Lett.* **119** 176809
- [10] Zhang L, Dolev M, Yang Q I, Hammond R H, Zhou B, Palevski A, Chen Y and Kapitulnik A 2013 *Phys. Rev. B* **88** 121103

- [11] Bedanta S, Barman A, Kleemann W, Petravic O and Seki T 2013 *J. Nanomater.* **2013** 952540
- [12] Ruderman M A and Kittel C 1954 *Phys. Rev.* **96** 99
- [13] Kasuya T 1956 *Prog. Theor. Phys.* **16** 45
- [14] Yosida K 1957 *Phys. Rev.* **106** 893
- [15] McGuire T R and Shafer M W 1964 *J. Appl. Phys.* **35** 984
- [16] Oveshnikov L N, Prudkoglyad V A, Selivanov Yu G, Chizhevskii E G and Aronzon B A 2017 *JETP Lett.* **106** 526
- [17] Aronzon B A, Oveshnikov L N, Prudkoglyad V A, Selivanov Y G, Chizhevskii E G, Kugel K I, Karateev I A, Vasiliev A L and Lähderanta E 2018 *J. Magn. Magn. Mater.* **459** 331
- [18] Abrikosov A A 1980 *Adv. Phys.* **29** 869
- [19] Kurilovich P D, Kurilovich V D and Burmistrov I S 2016 *Phys. Rev. B* **94** 155408
- [20] Analytis J G, Chu J-H, Chen Y, Corredor F, McDonald R D, Shen Z X and Fisher I R 2010 *Phys. Rev. B* **81** 205407
- [21] Furdyna J K 1988 *J. Appl. Phys.* **64** R29
- [22] Smit J 1966 *J. Appl. Phys.* **37** 1455
- [23] Soellinger W, Heiss W, Lechner R T, Rumpf K, Granitzer R, Krenn H and Springholz G 2010 *Phys. Rev. B* **81** 155213
- [24] Yamada K and Kamata N 1992 *J. Magn. Magn. Mater.* **104-7** 991
- [25] Yamada K, Satoh K, Kowata A and Yamaguchi K 1995 *J. Magn. Magn. Mater.* **140-4** 2047
- [26] Serral Gracia R, Nieuwenhuizen Th M and Lerner I V 2004 *Europhys. Lett.* **66** 419
- [27] Nieuwenhuizen Th M 1993 *Europhys. Lett.* **24** 797
- [28] Kulbachinskii V A, Miura N, Nakagawa H, Arimoto H and Ikaida T 1999 *Phys. Rev. B* **59** 15733
- [29] Kulbachinskii V A, Kytin V G, Kudryashov A A, Lunin R A and Banerjee A 2017 *Low Temp. Phys.* **43** 454
- [30] Kudryashov A A, Kytin V G, Lunin R A, Kulbachinskii V A and Banerjee A A 2016 *Semiconductors* **50** 869
- [31] Hsieh D et al 2009 *Nature* **460** 1101
- [32] Oveshnikov L N, Prudkoglyad V A, Nekhaeva E I, Kuntsevich A Y, Selivanov Y G, Chizhevskii E G and Aronzon B A 2016 *JETP Lett.* **104** 629